
01 Jul 2016

Hydrothermal Synthesis and Characterisation of Bioactive Glass-Ceramic Nanorods

Ehsan Zeimaran


Sara Pourshahrestani

Seyed Farid Seyed Shirazi

Belinda Pinguan-Murphy

et. al. For a complete list of authors, see https://scholarsmine.mst.edu/che_bioeng_facwork/1108

Follow this and additional works at: https://scholarsmine.mst.edu/che_bioeng_facwork

 Part of the [Biochemical and Biomolecular Engineering Commons](#), and the [Biomedical Devices and Instrumentation Commons](#)

Recommended Citation

E. Zeimaran et al., "Hydrothermal Synthesis and Characterisation of Bioactive Glass-Ceramic Nanorods," *Journal of Non-Crystalline Solids*, vol. 443, pp. 118 - 124, Elsevier, Jul 2016.

The definitive version is available at <https://doi.org/10.1016/j.jnoncrysol.2016.04.005>

This Article - Journal is brought to you for free and open access by Scholars' Mine. It has been accepted for inclusion in Chemical and Biochemical Engineering Faculty Research & Creative Works by an authorized administrator of Scholars' Mine. This work is protected by U. S. Copyright Law. Unauthorized use including reproduction for redistribution requires the permission of the copyright holder. For more information, please contact scholarsmine@mst.edu.



Hydrothermal synthesis and characterisation of bioactive glass-ceramic nanorods



Ehsan Zeimaran^a, Sara Pourshahrestani^a, Seyed Farid Seyed Shirazi^{a,b}, Belinda Pinguan-Murphy^a, Nahrizul Adib Kadri^{a,*}, Mark R. Towler^{a,c,**}

^a Department of Biomedical Engineering, Faculty of Engineering, University of Malaya, Kuala Lumpur 50603, Malaysia

^b Department of Mechanical Engineering, Faculty of Engineering, University of Malaya, Kuala Lumpur 50603, Malaysia

^c Department of Mechanical & Industrial Engineering, Ryerson University, Toronto, M5B 2K3, ON, Canada

ARTICLE INFO

Article history:

Received 5 February 2016

Received in revised form 31 March 2016

Accepted 2 April 2016

Available online 22 April 2016

Keywords:

Bioactive glass-ceramic

Nanorod

Hydrothermal treatment

Sol-gel

Bioactivity

ABSTRACT

In this study fabrication of rod-like bioactive glass-ceramics (BGCs) using hydrothermal treatment based on a sol-gel precursor is reported for the first time. BGCs with composition 58 wt% SiO₂, 33 wt% CaO and 9 wt% P₂O₅ were synthesized in different thermal conditions (200 and 220 °C) and characterised with regard to morphology, chemical composition and crystallinity. The bioactivity of the materials was assessed by immersion in simulated body fluid for up to 7 days. The results revealed that as the reaction temperature increased from 200 to 220 °C, the diameter of rods was reduced from microscale to nanoscale and the crystallinity was enhanced. It was also found that the BGC nanorods have higher surface area and consequently enhanced bioactivity than BGC microrods. This technique provides a facile method for rapid production of BGC nanorods at relatively low temperature which may have the potential to be used as bioactive composite reinforcement or for bone grafting applications.

© 2016 Elsevier B.V. All rights reserved.

1. Introduction

Bioactive glasses have been evaluated for maxillofacial and musculo-skeletal, drug delivery and hemostatic applications since their discovery in 1969 [1–5]. Bioactive glasses are capable of forming an interfacial bond to bone through rapid formation of hydroxyl carbonate-apatite on the surface upon implantation which promotes cell migration and differentiation [6]. The ability of bioactive materials to release ions into the surrounding environment can stimulate the healing process at the site of injury [7–9]. The mechanical and biological characteristics of bioactive glasses are markedly influenced by material properties such as particle size, morphology and chemical composition [10,11].

There has been growing interest in developing bioactive glass/ceramic materials on the nano-structural level due to their enhanced bioactivity resulting from the increased surface area [12], which leads to a greater dissolution rate [11]. Furthermore, controlling the size and shape of nanoparticles is crucial with respect to their interaction with cells [13]. Bioactive glass/ceramic nanoparticles can be used as reinforcement in polymer-inorganic nanocomposites [14]. In tissue

engineering scaffolds, using anisotropic structures such as elongated particles or fibers is preferred to spherical particles since they better mimic the native extracellular matrix (ECM). Unal et al. reported that needle-like inorganic particles can influence the mechanical properties of polymer-inorganic composites significantly more than spherical fillers [15]. Okuda et al. also found that when rod-like particles of hydroxyapatite (HA) were implanted in bone defects in rabbit femurs, they integrated more quickly into bone than globular-shaped particles [16]. Thus, the assembly of nanoparticles with novel structures and high length-diameter ratios, such as rod-like, needle-like or wire-like particles is a research area with much potential.

Recently, rod-like bioceramics have been prepared by various techniques such as sonochemical [17], coprecipitation [18], sol-gel [19], and hydrothermal [20] methods. The latter is a typical process for synthesizing inorganic materials with good repeatability. The main advantage of hydrothermal synthesis over other non-conventional ceramic synthesis methods such as sol-gel, is in producing ceramic bodies at relatively low temperatures (under 300 °C). The compression of samples under hydrothermal conditions accelerates densification of inorganic materials and allows better control of crystallization, purity and even morphology of the products [21]. To the authors' knowledge no study has yet reported the fabrication of nanorod-like bioactive glass-ceramics (BGC) using a hydrothermal method.

Here, we report the synthesis of rod-like sol-gel derived BGCs based on SiO₂-CaO-P₂O₅ by means of a hydrothermal method. Two

* Corresponding author.

** Correspondence to: M.R. Towler Department of Mechanical & Industrial Engineering, Ryerson University, Toronto, M5B 2K3, ON, Canada.

E-mail addresses: nahrizuladib@um.edu.my (N.A. Kadri), mtowler@ryerson.ca (M.R. Towler).

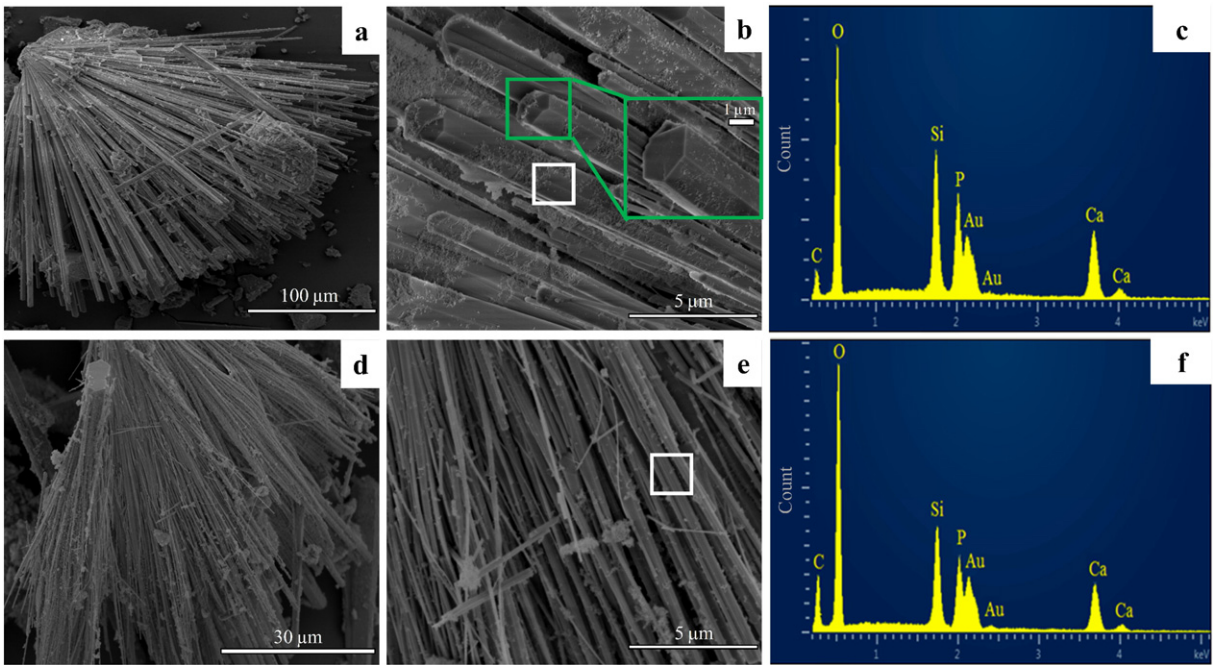


Fig. 1. FESEM micrographs of the BGC rods synthesized at 200 °C (a, b); at 220 °C (d, e) at two different magnifications (the inset shows the hexagonal structure of microrods) and the corresponding EDX spectra (c, f). FESEM images show the area for EDX analysis as indicated by white square line.

different temperatures (i) 200 °C and (ii) 220 °C were selected for hydrothermal treatment and the influence of temperature on crystallization and other structural changes was investigated. Finally,

the impact of these variables on the bioactive response of the synthesized materials was assessed after soaking in simulated body fluid (SBF) solution at 37 °C.

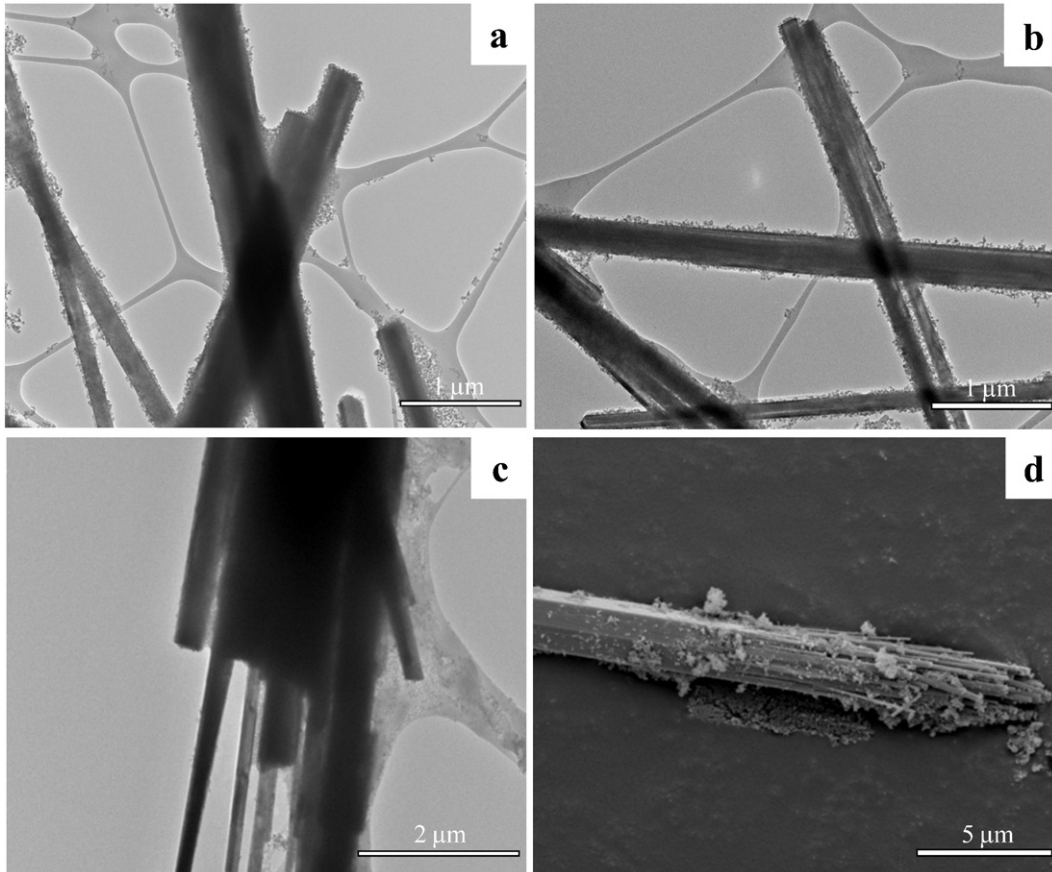


Fig. 2. TEM micrographs of synthesized BGC rods at (a) 200 °C and (b) 220 °C. TEM (c) and FESEM (d) images of a microrod started to grow from centre after 12 h of reaction.

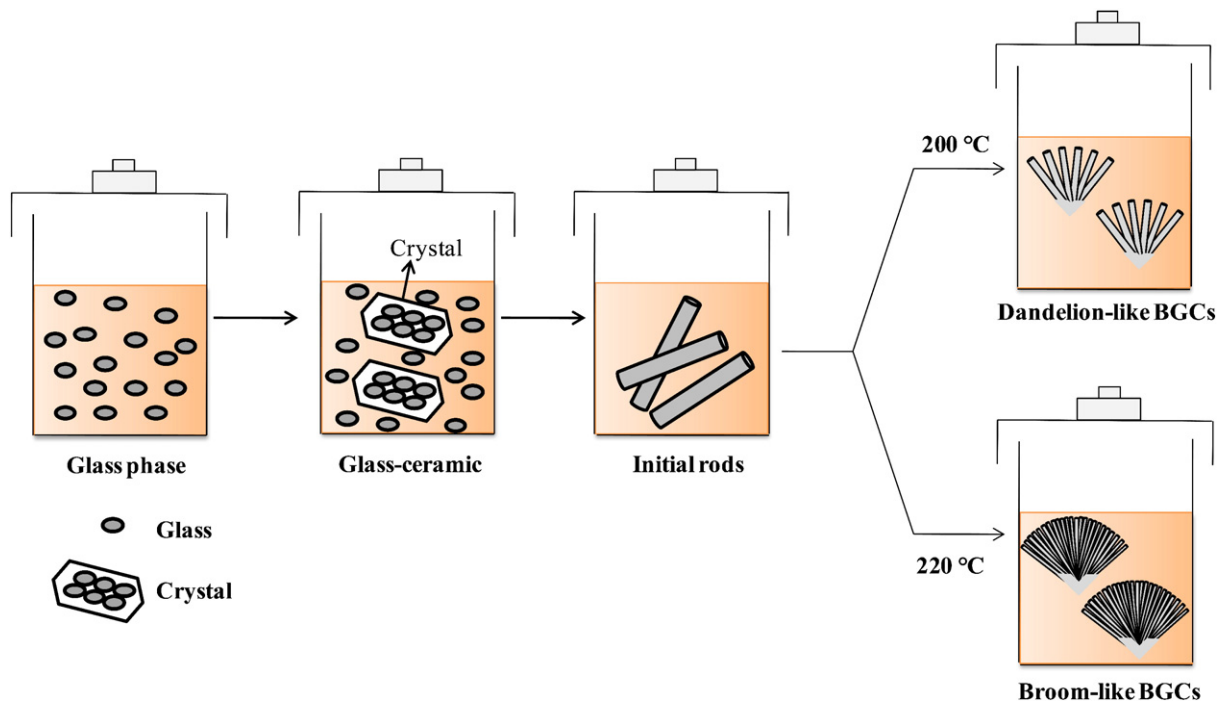


Fig. 3. Schematic illustration of the shape-controlled synthesis of dandelion and broom-like particles of BGCs by a hydrothermal route.

2. Experimental

2.1. Fabrication of bioactive glass ceramic (BGC) rod

A bioactive glass-ceramic with a composition of 58 wt% SiO₂–33 wt% CaO–9 wt% P₂O₅ was synthesized by the hydrothermal method. The reagents used for the preparation of the sol were purchased from Sigma-Aldrich (USA), with high purity ($\geq 98\%$). Initially, 8.62 mL of tetraethoxysilane (TEOS) was added to 30 mL of 0.1 N HNO₃ aqueous solution and the mixture was allowed to react for 1 h for the complete hydrolysis of TEOS. Then, 0.86 mL of triethylphosphate (TEP) and 5.55 g calcium nitrate tetrahydrate were added to the above solution in sequence and allowed 45 min for each reagent to completely react. Then, the obtained sol was transferred into a 60 mL Teflon-lined stainless-steel autoclave. After sealing, the autoclave was heated in an oven for 24 h. The hydrothermal treatment was performed at two different temperatures of 200 and 220 °C in order to investigate the effect of temperature on morphology and physical properties of synthesized materials, hereafter we name the samples BGC200 and BGC220, respectively. After the autoclave was naturally cooled to room temperature, the suspension was separated by centrifugation, washed with ethanol and distilled water several times, and dried at 100 °C overnight.

2.2. Structural characterisation

The microstructures and morphology of the samples were observed by field emission scanning electron microscopy (FESEM: Quanta™ 250 FEG–FEI, USA) and transmission electron microscopy (TEM, Hitachi, HT-7700, Japan). The rod diameters were measured manually from FESEM micrographs using ImageJ software (NIH, Bethesda, MD) by analysis of 10 individual particles for each sample. Elemental analysis was performed by energy dispersive spectroscopy (EDX: 20 mm X-Max, Oxford Instruments, Oxford, UK) attached to the FESEM. X-ray diffraction (XRD) patterns were obtained using an X-ray diffractometer (PANalytical Empyrean) with Cu K α radiation. FTIR analysis was conducted in a Perkin-Elmer Spectrum 400 spectrometer using the KBr pellets technique. The specific surface area, pore volume and pore size distribution of the samples were determined by Brunauer–

Emmett–Teller (BET) and Barret–Joyner–Halenda (BJH) analyses, with a Micromeritics ASAP 2020.

2.3. In vitro bioactivity study

The apatite-forming abilities of BGCs were investigated by their immersion in SBF, prepared in accordance with the protocol described by Kokubo and Takadama [22]. The samples (2.5 mg/mL) were incubated in SBF at 37 °C for 1 and 7 days. At each time point, the BGCs were removed from SBF, gently rinsed with distilled water and oven dried at 60 °C. The newly formed apatite layers on the surface of the BGC rods were analyzed by FESEM, XRD and FTIR.

3. Results and discussion

3.1. Structural characterisations of rod-shaped BGCs

Fig. 1 shows FESEM images and corresponding EDX spectra of rod-like BGCs synthesized by the hydrothermal method at 200 and 220 °C for 24 h. The results indicated that micron size particles with dandelion and broom-shaped structures with arranged rods were obtained at 200

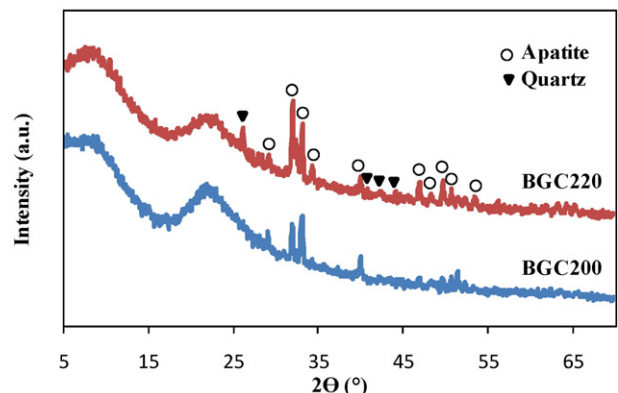


Fig. 4. XRD patterns of synthesized rod-like BGCs.

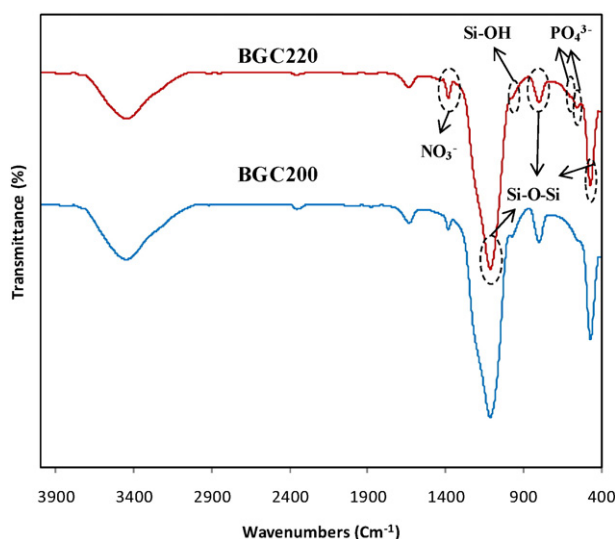


Fig. 5. FTIR spectra of synthesized rod-like BGCs.

and 220 °C, respectively. The rods prepared at 200 °C mainly have a hexagonal cylinder morphology and as the temperature increased the rod diameters shifted from micron (few hundred nm to 6.9 μm) to nano size (76 to 650 nm) and the size of rods become more uniform with mainly circular cylinder rod-like morphology. However the rod length was not obviously changed. EDX analysis of rods (Fig. 1c, f) confirmed the ternary system of the BGCs, containing the elements silicon, calcium and phosphorous.

The synthesized rod-like BGCs were subjected to TEM analysis to determine their geometry (Fig. 2a, b). The results demonstrated that rod-like BGCs have smooth surfaces. In addition, the sample that was prepared at 200 °C was composed of a wide range of diameters while the sample synthesized at 220 °C was more uniform. Furthermore, it showed that sample BGC200 was formulated of rods with larger diameters than BGC220 (in line with the FESEM observations). To further evaluate microbroom formation a sample synthesized at 200 °C for 12 h was observed under FESEM and TEM (Fig. 2c, d). After 12 h, only a small amount of the product was obtained. The corresponding images illustrate the beginning of multiple rods growth from an initial formed rod.

The formation of the 3D-structured dandelion and broom-like BGCs is proposed based on the experimental results, as shown in Fig. 3. The formation process includes nucleation, splitting growth, and formation of rod-like structures. Indeed, the nuclei were firstly evolved into single microrods and secondly by increasing the reaction time, microrods converted into dandelion-like structures by multiple rod growth from the centre of an initial rod. Finally, at 220 °C, the rods that formed the dandelion structures grew further into broom-like structure composed of nanorods via splitting. It is well-known that crystal structure of minerals

affect on their splitting ability [23]. Thus, in our experiment raising the reaction temperature from 200 to 220 °C enhanced the degree of crystal splitting and shifted the microrods to nanorods.

Fig. 4 shows the XRD patterns of prepared rod-like BGCs. The results show that the materials are partially crystallized and consist of both crystalline and amorphous parts. The growth of the amorphous phase can be related to the presence of silicon which disturbed crystalline formation, especially at the lower temperature. In comparison to BGC220, BGC200 exhibits smaller degree of crystallinity. Some crystal diffraction peaks appeared in the patterns (2θ ; 29.2, 31.8, 33.2, 34.4 and 40.4°) which could be assigned to the crystallization of calcium phosphate (CaP, JCPDS 024-0033). As the temperature increased to 220 °C new peaks appeared (2θ ; 26.2, 40.8, 42.7 and 45°) which could be ascribed to the crystallization of silicate into quartz (SiO_2 , JCPDS 07-0346) [24]. This confirms that the crystallinity of BGC rods could be increased in line with reaction temperature. The diffractogram for BGC220 indicates the presence of both crystalline apatite and quartz.

Fig. 5 shows FT-IR adsorption spectral curves of the BGCs rods prepared at different temperatures. The spectra of both samples are dominated by a strong signal related to nitrate ions at 1360 cm^{-1} which are often present in sol-gel derived bioactive glasses as a result of using HNO_3 as a catalyst in the synthesis procedure [25]. The small peak at about 461 cm^{-1} is ascribed to the Si—O—Si bending vibration while the peak at 787 cm^{-1} is attributed to the Si—O—Si symmetric stretching, and the strong absorption band at 1103 cm^{-1} is assigned to the Si—O—Si asymmetric stretching [26,27]. Further, the band at 966 cm^{-1} is ascribed to the stretching modes of Si—OH, confirming the presence of non-bridging oxygen in the matrix. The wide peaks located at 3423 and 1614 cm^{-1} could be due to the stretching vibration of the H—O bond of H_2O that was absorbed in the materials. Comparison of both spectra revealed that increasing reaction temperature led to splitting of the band at 570 cm^{-1} attributed to the bending vibration of amorphous P—O into two small bands at 554 and 603 cm^{-1} indicating the bending vibration of P—O bond in crystal phosphate as well as a decrease in intensity of the band at 966 cm^{-1} for non-bridging oxygens [28]. These results indicate that the crystallinity of BGC rods enhanced with increasing hydrothermal temperature which is consistent with the results of XRD analysis.

The N_2 adsorption-desorption isotherms and the Barrett-Joyner-Halenda (BJH) pore size distribution for the both BGC200 and BGC220 are plotted in Fig. 6. The specific surface areas as obtained by the BET method, BJH total pore volume and BJH average pore diameter are listed in Table 1. As can be seen in Fig. 6a, both samples showed type IV isotherm patterns with H3-type hysteresis loops that is characteristic of mesoporous materials with slit-shape pores according to IUPAC classification [29]. In contrast to BGC200, for the BGC220 adsorption isotherm, the hysteresis loop is much larger indicating a higher overall mesopore volume. Fig. 6b confirms that both samples have a broad pore size distribution in the mesopore range ($2\text{ nm} < \text{pore diameter} < 130\text{ nm}$). Apparently, BGC220 exhibited narrower pore size distribution than BGC200. The BGC220 had higher surface area than BGC200 which could be

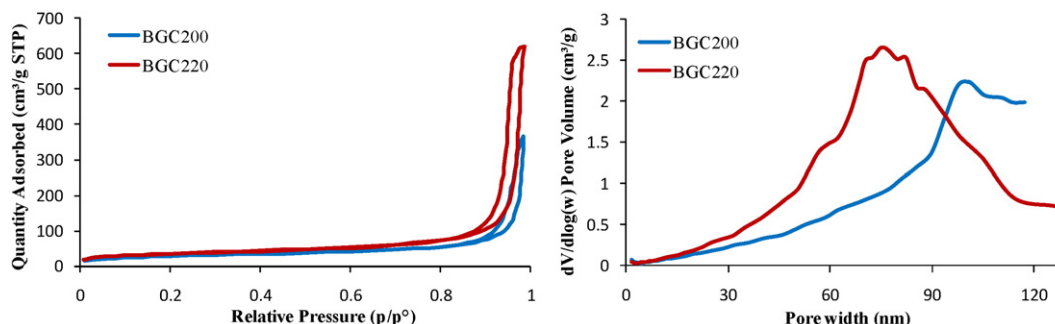


Fig. 6. (a) N_2 adsorption-desorption isotherms and (b) pore size distributions obtain from BJH analysis of the synthesized rod-like BGCs.

Table 1
N₂ adsorption/desorption parameters of the synthesized BGC rods.

Sample code	Surface area (m ² /g)	Average pore width (nm)	Pore volume (cm ³ /g)
BGC200	103.92	27.77	0.55
BGC220	130.93	33.96	0.94

attributed to the nanostructure of BGC220. Furthermore, the pore volume of BGC220 is significantly higher than BGC200, 0.96 and 0.56 cm³g⁻¹, respectively.

It is established that smaller bioactive glass particles with higher specific surface area accelerate the mineralization process of HA [11]. It is also well known that by increasing the degree of crystallinity a certain decrease in the bioactive response would take place [24]. Therefore, in this study we have further investigated the apatite-forming ability of materials to have a better understanding of the effect of both surface area and degree of crystallinity on the bioactive response.

3.2. *In vitro* bioactivity test

The *in vitro* bioactivity of BGC rods was investigated by soaking the samples in SBF for periods of 1 and 7 days. Fig. 7 illustrates representative FESEM images and EDX spectra of the materials' surfaces after soaking in SBF. The results showed that both samples have excellent apatite-forming ability. Compared to surface morphology before soaking, a new apatite layer with an appreciable thickness formed on the surfaces of both samples after 1 day immersion in SBF. The apatite layers were further thickened in the FESEM images (Fig. 7b) after 7 days of incubation period and filled the space between the rods. Although it is reported that crystallization of bioactive glasses decreases bioactivity [28], a greater amount of HA was observed on the surface of nanorods as compared to microrods. Therefore, the larger surface area of nanorods could be a controlling factor for accelerated apatite deposition.

The EDX analysis of the formed apatite layers show a higher concentration of Ca and P relative to that of Si after soaking in SBF (Fig. 7). The results demonstrated a significant decrease in Si content while the

concentration of Ca and P increased compared to the precursor materials (Fig. 1), which strengthens the indication of the formation of an apatite layer on the surface of samples. The Ca/P atomic ratio was approximately 1.46 and 1.54 for BGC200 and BGC220, respectively, which are close to those of stoichiometric HA (1.67).

The nature of the apatite layer formed on the surface of BGC rods was further examined by XRD (Fig. 8). In comparison to BGC200 before soaking in SBF, the intensity of diffraction peaks in the initial sample reduced or disappeared and the peaks associated with HA were less obvious after 1 day incubation. After 1 day, the apatite phase could not be detected, possibly due to the reaction with SBF and formation of amorphous silica on the surface [30]. In the next stage, Ca²⁺ and PO₄³⁻ ions migrate through the silica-rich layer causing the growth of CaP. Thus, after prolonged incubation (7 days), the peaks corresponding to CaP can be seen at 2θ = 26°, 2θ = 32° and 2θ = 46.8° [30,31]. However, this is a very early stage of HA precipitation with very low crystallinity.

In the case of nanorods, the crystalline peaks of apatite and quartz were intensified after 1 day soaking in SBF and prolonged incubation time resulted in a small decrease in peak intensities but still remained strong. This result is in agreement with study by Padilla et al. demonstrating that the diffraction peaks of crystalline ternary bioactive glass-ceramic (70S26C4P) treated at high temperature were still presented after 7 day soaking in SBF [24].

FTIR spectroscopy was performed to determine the difference in *in vitro* bioactivity after soaking in SBF for different times, as shown in Fig. 9. The results revealed that after 7 days of immersion, the adsorption peak at 1360 cm⁻¹ related to nitrate anions disappeared for both BGCs and some characteristic peaks of crystalline HA appeared. As can be seen in BGC200 spectra (Fig. 9a), the small adsorption peak at 570 cm⁻¹ attributed to amorphous P—O was unchanged after 1 day immersion but intensified after 7 days and two new peaks at 1455 and 1535 cm⁻¹ for the adsorption of carbonated groups appeared. After 1 day immersion, a small variation in the band shape at 1103 cm⁻¹ was observed as well as a shift towards lower wave numbers; these variations could be due to the appearance of a P—O anti-symmetric stress band at 1091 cm⁻¹ indicating the formation of CaP [32]. After a prolonged soaking time of 7 days, the peak at 570 cm⁻¹ attributed to P—O bond was intensified indicating the formation of poorly crystalline

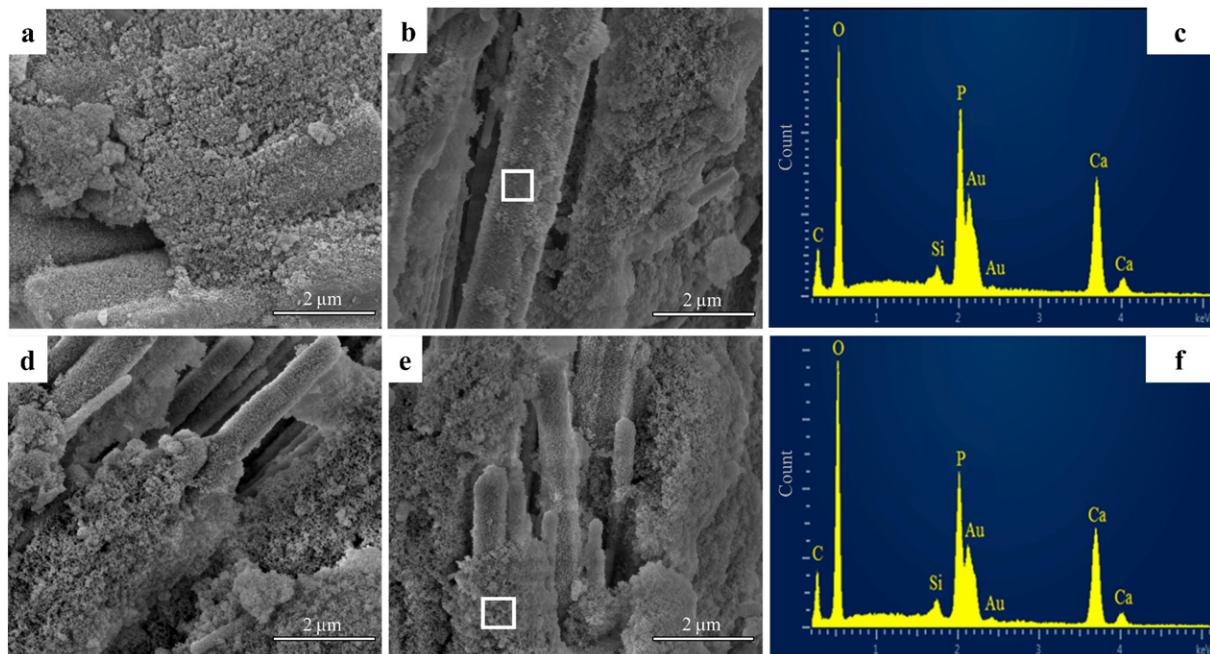


Fig. 7. FESEM micrographs of the samples after soaking in SBF: (a) BGC200 after 1 day; (b) BGC200 after 7 days; (c) BGC220 after 1 day and (d) BGC220 after 7 days and their corresponding EDX after 7 days; the square white line on the rods is the area analyzed by the EDX.

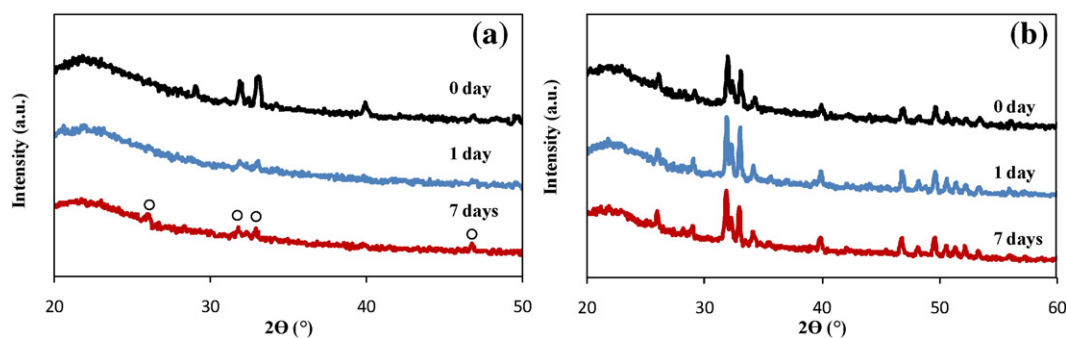


Fig. 8. XRD patterns of (a) BGC200 (b) BGC220; before and after 1 and 7 day immersion in SBF. (o) Apatite.

apatite at this early stage of immersion, in agreement with XRD results. BGC220 (Fig. 9b) showed double bands at 554 and 603 cm^{-1} assigned to crystalline CaP or apatite after 1 day soaking in SBF and intensified by incubation time. The bands relating to carbonate (1455 and 1535 cm^{-1}) were also observed for the BGC220 after 1 day incubation in SBF. Furthermore, the band at 966 cm^{-1} assigned to Si—OH groups overlapped with the bands corresponding to Si—O—Si and PO_4^{3-} groups at 1095 cm^{-1} and increased in size after 7 days indicating the formation of more CaP. Indeed, the band at 1103 cm^{-1} shifted to 1095 cm^{-1} which could be due to the formation of crystalline CaP. The FTIR results confirmed the formation of CaP on both BGCs.

Better osteoconductivity upon implantation of an orthopaedic device can be achieved if that device resembles the surrounding tissue in composition and morphology [33]. Attention has been paid to developing nanoscale biomaterials for biomedical applications because of their features that mimic the extracellular matrix (ECM). Indeed, bioactive glass particles on the nanoscale not only accelerate the mineralization process of HA but also improve biocompatibility and protein adsorption in comparison to the particles in microscales [11]. Nanoscale bioactive glass-ceramics with spherical and rice-shaped structures have recently been fabricated by modification of the sol-gel method or combining the sol-gel method with a co-precipitation process [18,34]. However, high thermal treatment is required which results in relatively high energy consumption and may cause particle aggregation and can even turn a bioactive glass into an inert material. In this study, we

demonstrated that rod-like BGCs could be synthesized by a simple and green hydrothermal method at relatively low temperature. This process allows control of the BGC rod size and shape by manipulating temperature. The sizes of rods were decreased down to the nanoscale by increasing temperature. As a result the number of rods in a micro-broom increased which further led to enhancing the specific surface area, pore size and pore volume. Furthermore, increasing hydrothermal temperature resulted in improved crystallinity and induced the crystallization of two phases, apatite and quartz. Although crystallization of bioactive glasses would be expected to result in a decrease in bioactive response, the level of bioactivity of partially-crystallized glass-ceramics is reported to be equivalent to that of 45S5 Bioglass® when the mechanical properties of bioactive glass-ceramics is much closer to natural bone [35]. It is also well known that particles with higher surface area and pore volume would provide more nucleation sites for apatite formation. Thus, a small rod size and high specific surface area would enhance contact surface area with SBF and consequently improve bioactivity.

4. Conclusions

Ternary bioactive glass-ceramics ($\text{SiO}_2\text{-CaO-P}_2\text{O}_5$) with high silicon content were fabricated with dandelion and broom-like structures with rods sizes ranging from tens of nanometers to micrometers via the hydrothermal method. It was shown that morphology, size and crystallinity of BGCs could be controlled by manipulating reaction

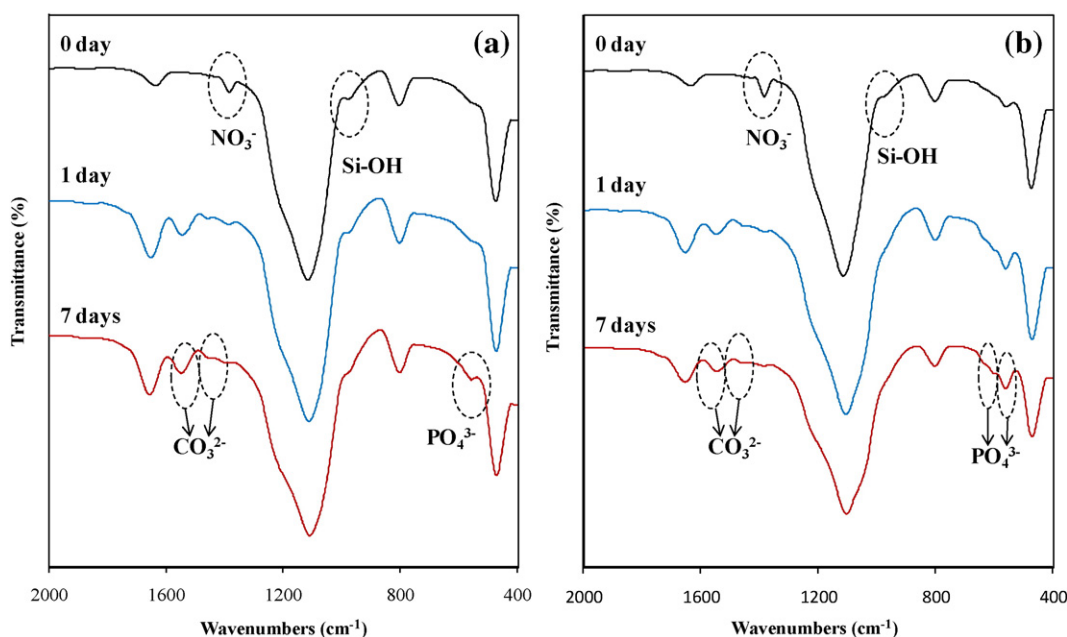


Fig. 9. FTIR spectra of (a) BGC200 and (b) BGC220; soaked in SBF for various periods.

temperature. An increase in the hydrothermal temperature from 200 to 220 °C led to a decrease in rod diameter from micro to nanoscale when at the same time the crystallinity and specific surface area were increased. *In vitro* bioactivity tests showed that the BGC rods could rapidly induce apatite deposition in SBF. The density of apatite formed on the surface of material was higher for the BGC nanorods than microrods. Therefore, using a facile hydrothermal method to synthesize BGCs not only reduces necessary synthesis temperature but also offers the opportunity to control morphology and crystallinity of products. The ability to produce BGCs with unique nanoscale morphology, high surface area and high bioactivity will open up new prospects in the development of biomaterials for clinical applications.

Acknowledgements

This research is supported by a High Impact Research Grant (UM.C/625/1/HIR/MOHE/ENG/58) from the Ministry of Higher Education Malaysia and University of Malaya Research Grant (UMRG, RG156-12AET).

References

- [1] L.L. Hench, R.J. Splinter, W. Allen, T. Greenlee, Bonding mechanisms at the interface of ceramic prosthetic materials, *J. Biomed. Mater. Res.* 5 (1971) 117–141.
- [2] M. Vallet-Regi, C. Ragel, A.J. Salinas, Glasses with medical applications, *Eur. J. Inorg. Chem.* 2003 (2003) 1029–1042.
- [3] S. Pourshahrestani, E. Zeimaran, N.A. Kadri, N. Gargiulo, S. Samuel, S.V. Naveen, T. Kamarul, M.R. Towler, Gallium-containing mesoporous bioactive glass with potent hemostatic activity and antibacterial efficacy, *J. Mater. Chem. B* 4 (2016) 71–86.
- [4] F.S. Shirazi, M. Mehrali, A. Ataollahi Oshkour, C. Metselaar, H. Simon, N.A. Kadri, A. Osman, N. Azuan, Characterization and mechanical properties of calcium silicate/citric acid-based polymer composite materials, *Int. J. Appl. Ceram. Technol.* 12 (2013) 371–376.
- [5] F.S. Shirazi, S. Gharehkhani, H.S.C. Metselaar, B. Nasiri-Tabrizi, H. Yarmand, M. Ahmadi, N.A.A. OSMAN, Ion size, loading, and charge determine the mechanical properties, surface apatite, and cell growth of silver and tantalum doped calcium silicate, *RSC Adv.* 6 (2015) 190–200.
- [6] J.R. Jones, Review of bioactive glass: from hench to hybrids, *Acta Biomater.* 9 (2013) 4457–4486.
- [7] E. Zeimaran, S. Pourshahrestani, B. Pingguan-Murphy, N.A. Kadri, H.A. Rothan, R. Yusof, M.R. Towler, I. Djordjevic, Fabrication and characterization of poly (octanediol citrate)/gallium-containing bioglass microcomposite scaffolds, *J. Mater. Sci.* 50 (2015) 2189–2201.
- [8] I.D. Xynos, A.J. Edgar, L.D. Buttery, L.L. Hench, J.M. Polak, Ionic products of bioactive glass dissolution increase proliferation of human osteoblasts and induce insulin-like growth factor II mRNA expression and protein synthesis, *Biochem. Biophys. Res. Commun.* 276 (2000) 461–465.
- [9] I.D. Xynos, A.J. Edgar, L.D. Buttery, L.L. Hench, J.M. Polak, Gene-expression profiling of human osteoblasts following treatment with the ionic products of Bioglass® 45S5 dissolution, *J. Biomed. Mater. Res.* 55 (2001) 151–157.
- [10] J.P. Fan, P. Kalia, L. Di Silvio, J. Huang, In vitro response of human osteoblasts to multi-step sol-gel derived bioactive glass nanoparticles for bone tissue engineering, *Mater. Sci. Eng. C* 36 (2014) 206–214.
- [11] A.A.R. De Oliveira, D.A. De Souza, L.L.S. Dias, S.M. De Carvalho, H.S. Mansur, M. de Magalhães Pereira, Synthesis, characterization and cytocompatibility of spherical bioactive glass nanoparticles for potential hard tissue engineering applications, *Biomed. Mater.* 8 (2013) 025011.
- [12] S.K. Misra, D. Mohn, T.J. Brunner, W.J. Stark, S.E. Philip, I. Roy, V. Salih, J.C. Knowles, A.R. Boccaccini, Comparison of nanoscale and microscale bioactive glass on the properties of P (3HB)/Bioglass® composites, *Biomaterials* 29 (2008) 1750–1761.
- [13] P. Kolhar, A.C. Anselmo, V. Gupta, K. Pant, B. Prabhakarpanandian, E. Ruoslahti, S. Mitragotri, Using shape effects to target antibody-coated nanoparticles to lung and brain endothelium, *Proc. Natl. Acad. Sci. U. S. A.* 110 (2013) 10753–10758.
- [14] E. Zeimaran, S. Pourshahrestani, I. Djordjevic, B. Pingguan-Murphy, N.A. Kadri, M.R. Towler, Bioactive glass reinforced elastomer composites for skeletal regeneration: a review, *Mater. Sci. Eng. C* 53 (2015) 175–188.
- [15] H. Unal, A. Mimaroglu, M. Alkan, Mechanical properties and morphology of nylon-6 hybrid composites, *Polym. Int.* 53 (2004) 56–60.
- [16] T. Okuda, K. Ioku, I. Yonezawa, H. Minagi, Y. Gonda, G. Kawachi, M. Kamitakahara, Y. Shibata, H. Murayama, H. Kurosawa, The slow resorption with replacement by bone of a hydrothermally synthesized pure calcium-deficient hydroxyapatite, *Biomaterials* 29 (2008) 2719–2728.
- [17] C. Qi, Y.-J. Zhu, X.-Y. Zhao, J. Zhao, F. Chen, G.-F. Cheng, Y.-J. Ruan, High surface area carbonate apatite nanorod bundles: surfactant-free sonochemical synthesis and drug loading and release properties, *Mater. Res. Bull.* 48 (2013) 1536–1540.
- [18] Z. Hong, E.G. Merino, R.L. Reis, J.F. Mano, Novel rice-shaped bioactive ceramic nanoparticles, *Adv. Eng. Mater.* 11 (2009) B25–B29.
- [19] S.K. Padmanabhan, A. Balakrishnan, M.-C. Chu, Y.J. Lee, T.N. Kim, S.-J. Cho, Sol-gel synthesis and characterization of hydroxyapatite nanorods, *Particuology* 7 (2009) 466–470.
- [20] X.-Y. Zhao, Y.-J. Zhu, F. Chen, B.-Q. Lu, C. Qi, J. Zhao, J. Wu, Hydrothermal synthesis of hydroxyapatite nanorods and nanowires using riboflavin-5'-phosphate monosodium salt as a new phosphorus source and their application in protein adsorption, *CrystEngComm* 15 (2013) 7926–7935.
- [21] M. Yoshimura, K. Byrappa, Hydrothermal processing of materials: past, present and future, *J. Mater. Sci.* 43 (2008) 2085–2103.
- [22] T. Kokubo, Apatite formation on surfaces of ceramics, metals and polymers in body environment, *Acta Mater.* 46 (1998) 2519–2527.
- [23] J. Tang, A.P. Alivisatos, Crystal splitting in the growth of Bi₂S₃, *Nano Lett.* 6 (2006) 2701–2706.
- [24] S. Padilla, J. Roman, A. Carenas, M. Vallet-Regi, The influence of the phosphorus content on the bioactivity of sol-gel glass ceramics, *Biomaterials* 26 (2005) 475–483.
- [25] M. Catauro, F. Bollino, R. Renella, F. Papale, Sol-gel synthesis of SiO₂-CaO-P₂O₅ glasses: influence of the heat treatment on their bioactivity and biocompatibility, *Ceram. Int.* 41 (2015) 12578–12588.
- [26] J. Ma, C. Chen, D. Wang, X. Meng, J. Shi, Influence of the sintering temperature on the structural feature and bioactivity of sol-gel derived SiO₂-CaO-P₂O₅ bioglass, *Ceram. Int.* 36 (2010) 1911–1916.
- [27] F. Shirazi, M. Mehrali, B. Nasiri-Tabrizi, S. Baradaran, S. Gharehkhani, H. Metselaar, N. Kadri, N. Osman, Mechanochemical synthesis and characterization of silver (Ag⁺) and tantalum (Ta⁵⁺) doped calcium silicate nanopowders, *Sci. Adv. Mater.* 7 (2015) 2664–2671.
- [28] Z. Hong, R.L. Reis, J.F. Mano, Preparation and in vitro characterization of novel bioactive glass ceramic nanoparticles, *J. Biomed. Mater. Res.* 88 (Part A) (2009) 304–313.
- [29] N. Coleman, L. Hench, A gel-derived mesoporous silica reference material for surface analysis by gas sorption 1. Textural features, *Ceram. Int.* 26 (2000) 171–178.
- [30] H. Pirayesh, J.A. Nychka, Sol-gel synthesis of bioactive glass-ceramic 45S5 and its in vitro dissolution and mineralization behavior, *J. Am. Ceram. Soc.* 96 (2013) 1643–1650.
- [31] X. Chen, B. Lei, Y. Wang, N. Zhao, Morphological control and in vitro bioactivity of nanoscale bioactive glasses, *J. Non-Cryst. Solids* 355 (2009) 791–796.
- [32] I. Izquierdo-Barba, A. Salinas, M. Vallet-Regi, In vitro calcium phosphate layer formation on sol-gel glasses of the CaO-SiO₂ system, *J. Biomed. Mater. Res.* 47 (1999) 243–250.
- [33] C. Du, F. Cui, X. Zhu, K. de Groot, Three-dimensional nano-HAp/collagen matrix loading with osteogenic cells in organ culture, *J. Biomed. Mater. Res.* 44 (1999) 407–415.
- [34] Z. Hong, A. Liu, L. Chen, X. Chen, X. Jing, Preparation of bioactive glass ceramic nanoparticles by combination of sol-gel and coprecipitation method, *J. Non-Cryst. Solids* 355 (2009) 368–372.
- [35] O. Peitl, E.D. Zanotto, F.C. Serbena, L.L. Hench, Compositional and microstructural design of highly bioactive P₂O₅-Na₂O-CaO-SiO₂ glass-ceramics, *Acta Biomater.* 8 (2012) 321–332.